Ionic and Poly(ionic liquid)s as Perovskite Passivating Molecules for Improved Solar Cell Performances

Silvia Mariotti, Daniele Mantione, Samy Almosni, Milutin Ivanović, Takeru Bessho, Miwako Furue, Hiroshi Segawa, Georges Hadziioannou, Eric Cloutet, Thierry Toupance

Ionic and Poly(ionic liquids) as Perovskite Passivating Molecules for Improved Solar Cell Performances

Silvia Mariotti,[a] Daniele Mantione,[a] Samy Almosni,[b] Milutin Ivanović,[a] Takeru Bessho,[b] Miwako Furue,[b] Hiroshi Segawa,[b*] Georges Hadziioannou,[a] Eric Cloutet,[a*] Thierry Toupance.[c*]

Perovskite solar cell devices have improved significantly in efficiency and are on the verge to commercialization. However, device stability has not yet been fully met. In this paper, we use a K^+-doped formamidinium (FA)-based perovskite, which has been shown to be an ideal perovskite composition for fabricating efficient solar cells with low hysteresis and better stability compared to MA-free perovskite materials. Nevertheless, in order to further progress on the device's performance and stability, additives were employed. While in the literature different types of additives have been used, in particular ionic liquids (ILs) and polymers, the novelty of this work lies in the use of *poly(ionic liquids)* (PILs) as additives for the absorber layer, which have been used only recently as perovskite passivation agent. The PILs were chosen for their high ionic conductivity and their hydrophobic nature in a macromolecular structure. Here we show a direct comparison between the performances of devices obtained by adding a passivation IL (tBMPy-TFSI) and its polymeric version PIL (PVMPy-TFSI) in the perovskite layer. Preliminary studies show that the addition of both additives promotes improved solar cell performances and reduces the degradation rate during measurement. In particular, while the IL mainly induces higher solar cell performances due to the increase in V_{OC} and FF, PIL promotes higher J_{SC}, performance stability under illumination and significantly reduces the *J-V* hysteresis index, to approach 0% under AM1.5G illumination. Thus, both ILs and PILs are valuable passivation molecules for perovskite grain boundaries, promoting charge diffusion and protecting the perovskite layer from external agents that may induce degradation. We believe that PIL additives present attractive prospects for stable perovskite solar cell devices.

1 Introduction

Since 2009, part of the photovoltaic community has shown a tremendous interest in perovskite materials for solar cell (SC) applications and achieved quickly outstanding device performances.[1,2,3] Today, only 13 years after their advent, perovskite solar cells (PSCs) have achieved up to 25.7% certified power conversion efficiency (PCE),[4,5] thus reaching similar performances to that of crystalline silicon (26.1%).[5] However, although industrial partners show great interest in such efficient and cheap alternative renewable energy source, the long-term stability of PSCs remains one of the main issues. In the last years, numerous studies concerning perovskite device stability have been reported in the literature, resulting in a great improvement of the device durability and thus bringing this technology very close to commercialization. However, there are still concerns about these devices being able to last as much as silicon solar cells (*i.e.* > 25 years), in particular because the most promising technology for future commercialization are perovskite/silicon tandem devices, made of a top perovskite solar cell and a bottom silicon solar cell, which up to date have achieved an efficiency of 29.8% by the Helmholtz Zentrum Berlin.[5] It is therefore a key requirement to reach similar life expectancy for both solar cells.

In order to improve the shelf life of PSCs, research groups have a) employed different encapsulation methods,[6] b) used alternative perovskite compositions,[7] c) studied methods for perovskite interfacial engineering, passivation and doping,[8,9] and d) used alternative transporting materials. For example, regarding the hole transporting material (HTM), work has been presented to replace 2,2',7,7'-Tetrakis[N,N-di(4-methoxyphenyl)amino]-9,9'-spirobifluorene (Spiro-OMeTAD) in n-i-p device architectures, obtaining higher environmental stability.[10,11] In addition, the stability of devices has been improved by using doping strategies for both HTM and the perovskite layer,[12,13,14] while recent studies focus on the perovskite passivation, by using additives which, not only help to improve the device stability, but also induce improved device performances.[15] In the literature, small molecules, including ionic liquids (ILs), and large molecules, such as polymers, have been employed as additives. Various small molecules (non-IL) additives were used in PSCs such as alkylphosphonic acid ω-ammonium chlorides,[16] thiophene and pyridine Lewis bases,[17] or quaternary alkyl ammonium cations.[18] In particular, Wu *et al.*

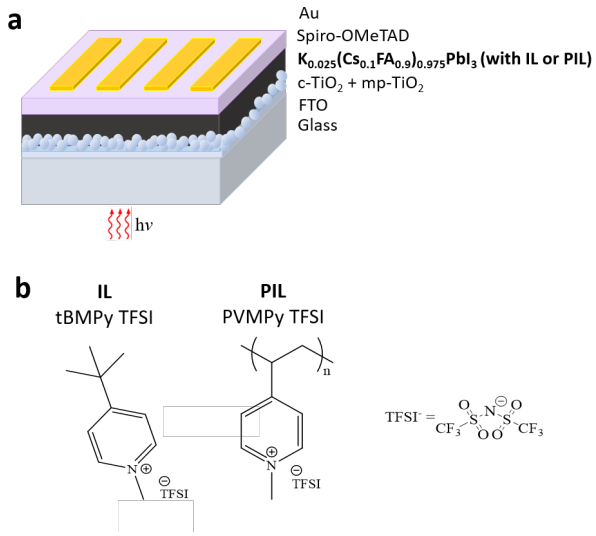

Fig. 1. a) Sketch of the n-i-p perovskite solar cell architecture and b) chemical structures of tBMPy-TFSI and PVMPy-TFSI.

have used pentaerythritol tetrakis(3-mercaptopropionate) (ML) spin-coated on top of the perovskite layer, to passivate uncoordinated Pb^{2+} and suppress the formation of Pb^0 defects, which are responsible for the poor performances of the device, in particular regarding the limited V_{OC}.[19] Alternatively, an increasing attention has been devoted to the use of molecular ILs.[20] The reason for this increased interest is that ILs exhibit several advantages such as high ionic conductivity, low vapor pressure, and excellent thermal and electrochemical stability which make them suitable candidates for controlling the growth of perovskite crystals, modifying interfaces, doping the perovskite and the hole transport material and improving the stability of PSCs.[21,22,23] For instance, regarding the absorber layer, Shahiduzzaman *et al.* have demonstrated that low concentrations of 1-hexyl-3-methylimidazolium chloride may improve the perovskite morphology and the light absorption.[24] Seo *et al.*, have shown that by adding methylammonium formate (MAF) they achieved highly oriented and pure perovskite crystals.[25] Doping the perovskite layer with 1-Butyl-3-methylimidazolium tetrafluoroborate ($BMIMBF_4$) also brought to a considerable improvement of the device stability, achieving a PCE loss of less than 5% under full illumination at c.a. 75°C for more than 1800 hours.[26] Finally, ILs were used as an interfacial layer between the electron transport layer (ETL) and the perovskite for enhancing device performance and/or stability.[27,28,29,30,31,32] It was shown that polar ILs induce a dipole formation at the charge transport/perovskite layer interface improving the energy level alignment owing to reduced interfacial energy barriers.

Polymer additives have been investigated too. For example, polyethylene glycol (PEG) and polymethyl methacrylate (PMMA), were used for controlled crystal growth and hence higher device performances.[33,34] In 2017, L. Zuo et al.[35] and B. Chaudhary[36] have shown that the pyridine group of hydrophobic poly(4-vinylpyridine) (P4VP) can passivate the uncoordinated Pb atoms on the perovskite surface, improving both the device efficiency and stability. Later, in 2019, T. Han *et al.*[37] used poly(propylene carbonate) (PPC) to dope the perovskite layer, using the Lewis-base polymer to crosslink the perovskite and enhance the device stability towards light, moisture, and heat. More recently, the modulation of both perovskite crystallization and electronic properties by adding a polymeric room-temperature molten salt yielded efficient and stable inverted PSCs.[38]

However, despite recent interest in poly(ionic liquid)s (PILs) in chemistry and material sciences, only a couple of studies deal with the use of poly(ionic liquids) (PILs) in PSCs. Compared to ILs, PILs give rise to better spatial control, show enhanced stability and durability while keeping good ionic conductivity.[39,40] In this context, in our previous work we have shown that PILs can be used as additives for the hole transporting material, in the form of poly(1-butyl-3-vinylimidazolium bis(trifluoromethylsulfonyl)imide) (PVBI-TFSI) and obtained higher device performances compared to devices using standard HTM doping.[41] Furthermore, improved stability and performance were recently reported for inverted p-i-n PSCs involving poly(1-ethyl-3-vinylimidazolium bis(trifluoromethyl-sulfonyl)imide) (PeIm-TFSI) as an interfacial layer between a triple cation perovskite film and a C_{60}-based ETL.[42] In this context, we herein demonstrate that PILs are efficient additives also for n-i-p formamidinium (FA)-based PSCs and we compare the corresponding device performances with those of solar cells doped with ILs. The study is performed on a potassium-doped FA-based perovskite with the following composition: $K_{0.025}(Cs_{0.1}FA_{0.9})_{0.975}PbI_3$. The potassium ($K^+$) doping is used to reduce the hysteresis of MA-free perovskite, as previously demonstrated by H. Segawa research group,[43] while the MA-free perovskite is chosen due to its improved device stability compared to the MA-based counterpart,[44] particularly due to better thermal and long-term stability. However, FA^+ cation being larger than MA^+, the pure $FAPbI_3$ perovskites shows thermodynamic instability, with fast transition towards a non-photoactive phase (δ-phase). This is prevented by adding small amounts of Cs^+, which however have a negative effect on operational stability and sensitivity towards humidity.[45] Addition of ILs and PILs in the perovskite layer allows passivation of the perovskite surface and protection against degrading factors, with particular regard to water. Hence, by taking advantage of all these features, the PSCs fabricated in this work show improved PCEs, insignificant hysteresis, and improved retention of PCE over time (by measuring maximum power point (MPP) under illumination). A typical perovskite n-i-p device architecture was selected for this scope, with the perovskite layer sandwiched between a TiO_2 ETL (compact and mesoporous) and a spiro-OMeTAD HTM layer, as shown in Fig. 1a. The perovskite layer was prepared by including additives (see SI, Section 4) in the precursor solution. The IL and PIL employed include tert-butyl methyl pyridinium and poly(vinyl methyl pyridinium) cationic units, and various counter-ions such as iodide (I^-), tetrafluoroborate (BF_4^-) or bis(trifluoromethane)sulfonimide ($TFSI^-$). For instance, chemical structures of tert-butyl methyl pyridinium bis(trifluoromethane) sulfonimide (tBMPy-TFSI) and poly(vinyl methyl pyridinium bis(trifluoromethane)sulfonimide) (PVMPy-TFSI) are shown in Fig. 1b. The cationic part is a quaternary

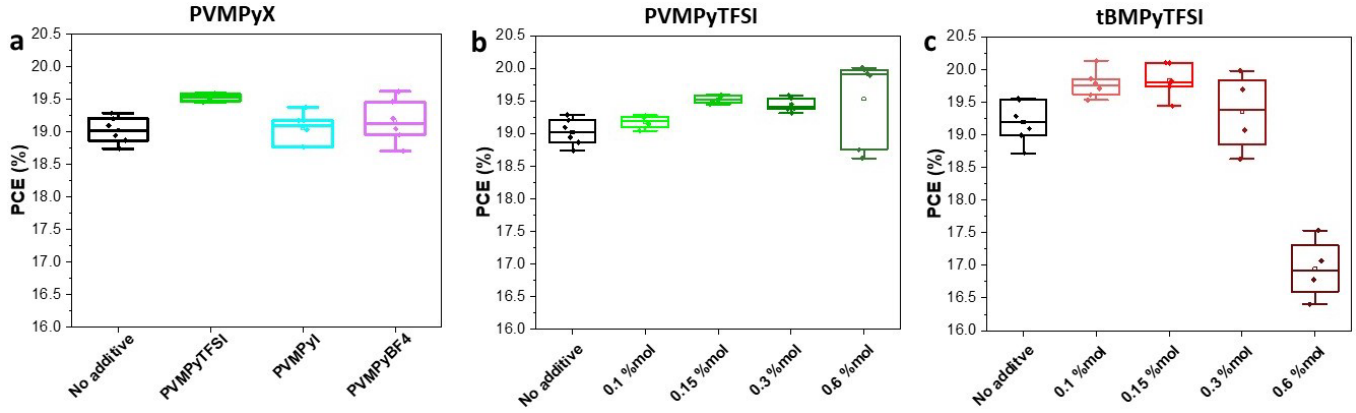

Fig. 2. a) PCE of devices containing PVMPy-based PILs with different anions (X). The optimized concentrations for each conditions are: PVMPyTFSI 0.15 %mol, PVMPyI 0.1 %mol, $PVMPyBF_4$ 0.1 %mol. Concentration series of b) PVMPYTFSI and c) tBMPyTFSI to define the optimized conditions for highest PCEs. For both PIL and IL the optimized concentration is 0.15 %mol.

ammonium (QAHs), which has proven to be a powerful passivation molecule as extensively shown in the literature.[46]

2 Results and discussion

The synthetic scheme of the different compounds, shown in Schemes S1 and S2 (SI), follows the typical two-steps pathway used for the preparation of ionic liquids.[39,47] First, an organic salt precursor is formed using the alkyl halide of the desired substituent: for this work iodomethane has been used to insert the methyl moiety on the nitrogen, leaving iodide ion as counter anion. The second step is an ion exchange, typically followed by the phase separation of the desired derivatives. Thus, lithium-TFSI was used in water as source of $TFSI^-$ anions, resulting in a quantitative precipitation of the desired ionic couple, for both IL and PIL (see SI, Sections 2 and 3). ^{1}H-NMR, ^{19}F-NMR and ^{13}C-NMR analyses confirm the formation of the two expected compounds for tBMPy-TFSI and PVMPyTFSI (Fig. S3-5 and Fig. S8-10 respectively). In particular, the AA'BB' pattern in the ^{1}H-NMR spectra belonging to the aromatic proton appears as two doublets in the case of the single-molecule and two wide signals in the case of the polymer, around 8 ppm. The methyl located on the nitrogen appears well-defined at about 4 ppm in both spectra and the protons of the tert-butyl group lead to a sharp signal at 1.2 ppm in the case of the IL. Finally, in the case of the PIL, the carbonaceous backbone is represented as group of signals at around 2.3 ppm. A similar strategy has been followed to prepare PVMPy-BF_4. Potassium tetrafluoroborate has been used to induce a precipitation in water of the exchanged iodide starting materials. The molecular weight of the PIL used is 60 kg/mol which showed higher solubility in the perovskite precursor solution compared to 120 kg/mol polymer analogue. Thus, the latter was not considered in the following.

For the device fabrication, three case scenarios were considered: i) pure perovskite solution (*i.e.* without additive), ii) perovskite with IL and iii) perovskite with PIL. First, the influence of the counter-anion nature in PIL on the photovoltaic performances was investigated. Although in the literature the main counter ions for alkyl ammonium passivating molecules are halides or BF_4^-,[26] we found that higher device PCEs and more stable MPP analysis are obtained using $TFSI^-$ as counter-ion instead of I^- and BF_4^-, as depicted in Fig. 2a and S12. The improved stability observed with $TFSI^-$ anion can be related to its highly hydrophobic nature that may be beneficial for the protection of the perovskite layer from humidity. Furthermore, using Density Functional Theory (DFT) calculations, P. Caprioglio *et al.* highlighted the presence of high interaction between nitrogen (from $TFSI^-$) and under coordinated lead atoms on the perovskite surface,[42] demonstrating that $TFSI^-$ is a suitable counter anion for perovskite passivation. As a result, only tBMPy-TFSI and PVMPy-TFSI were further investigated for the IL versus PIL comparison study. Indeed, their organic composition is very similar, the organic counter anion remains unchanged (bis(trifluoromethane)sulfonimide, $TFSI^-$) and the only difference concerns the macromolecular structure of PVMPy-TFSI polymer, compared to the tBMPy-TFSI molecular compound.

The influence of the additive amount in the perovskite layer was then evaluated for tBMPy-TFSI and PVMPy-TFSI. In both cases, the optimal concentration was found to be 0.15% mol, as indicated by the device performance studies as a function of additive concentration shown in Fig. 2, Fig. S13 and S14. In particular, Fig. S14 shows that higher PCEs can be obtained at higher concentrations (0.6 %mol), but the error bars indicate lower reproducibility. This can be attributed to PIL solubility issues at high concentrations, as shown in Fig. S11. Thus, the 0.15 mol% concentration was used as the optimized content since it led to high PCEs with excellent reproducibility. Fig. 3a shows the photovoltaic performances of the devices. While the average PCE for perovskite devices without additives reached 19.2%, the IL and PIL perovskite devices led to higher average efficiencies, *i.e.* 19.8% (± 0.33) and 19.5% (± 0.08) respectively. Not only does the efficiency of devices increase with the addition of IL and PIL additives, but the statistical error decreases, in particular for PVMPyTFSI, showing improved reproducibility. The higher device PCE is triggered by the increased V_{OC} and *FF* in the case of tBMPy-TFSI, and by the higher J_{SC} in the case of PVMPy-TFSI. The additives are assumed to saturate surface uncoordinated ionic sites, such as Pb^{2+} and I^- which have been classified as the main surface traps causing recombination.[48] The V_{OC} enhancement obtained with IL is a

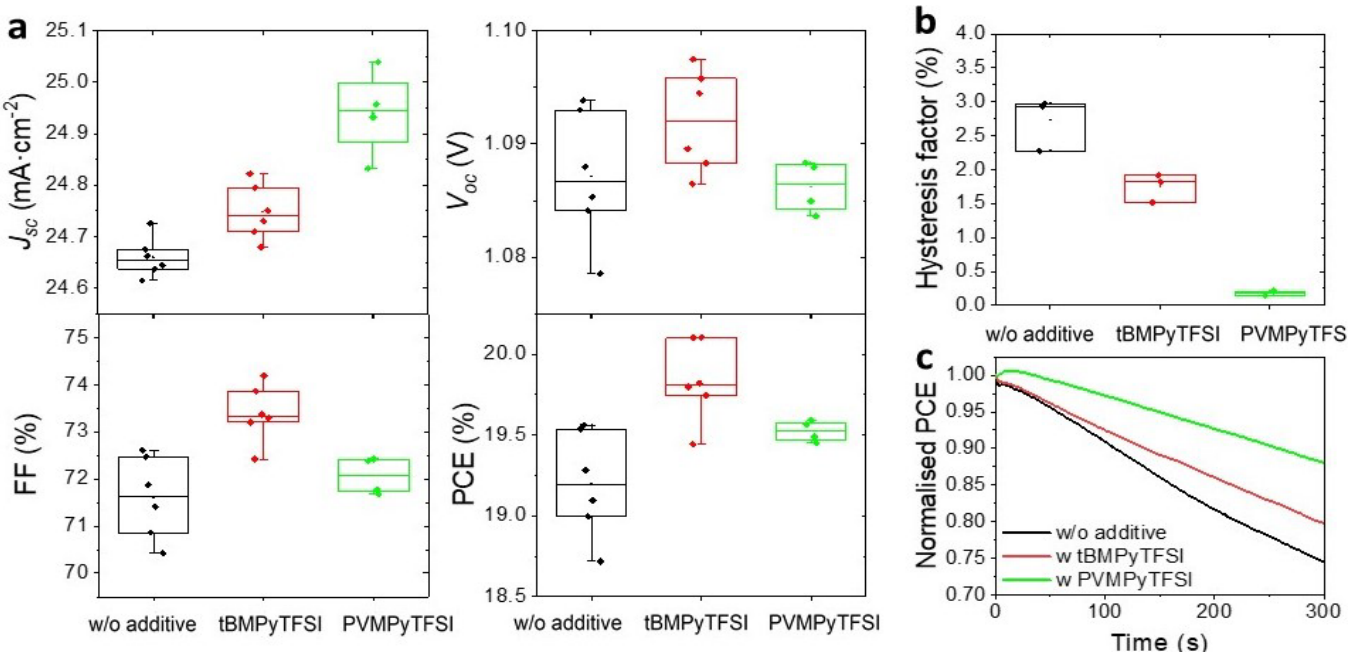

Fig. 3. a) *J-V* statistics of additive-free perovskite devices and with tBMPy-TFSI and PVMPy-TFSI, including J_{SC}, V_{OC}, FF and PCE. b) Hysteresis factor showing lower hysteresis for devices with IL and PIL and c) normalised PCE tracking under AM1.5 for 5 minutes.

consequence of the reduced charge recombination losses at the surface of perovskite layer as indicated by higher steady state photoluminescence (PL) (Fig. S15a). Furthermore, the J_{SC} enhancement found for PIL is related to faster charge extraction at TiO_2/perovskite and Perovksite/spiro-OMeTAD interfaces as revealed by the lower PL intensities measured for perovskite with PVMPy-TFSI (Fig. S15b and c). Representative *J-V* curves of these devices are shown in Fig. S16. No significant differences between forward and reverse scans are detected which is in agreement with the fact that hysteresis index (HI) of undoped $K_{0.025}(Cs_{0.1}FA_{0.9})_{0.975}PbI_3$ perovskite solar cells is typically low (< 3.5%) due to the K^+ perovskite doping.[43] Nevertheless, as shown in Fig. 3b, the hysteresis factor of devices with the perovskite containing IL and PIL additives further decreases. tBMPy-TFSI/perovskite devices show HI of 1.8%, whereas PVMPy-TFSI/perovskite devices produce *J-V* curves with HI as low as 0.2%. The reason for the reduced hysteresis in *J-V* curves of devices with perovskite including additives can be related to grain boundary passivation. Indeed, it is known that grain boundaries are responsible for trapping charge carriers, due to crystalline defects.[49] In addition, these imperfections are responsible for high recombination rates which largely contribute to hysteresis.[50] Therefore it can be assumed that additives such as ILs and PILs passivate the uncoordinated atoms, reducing the amount of traps, and hence contributing to a lower hysteresis factor. Specifically for tBMPyTFSI and PVMPyTFSI, *J-V* results show that the PIL is more efficient in doing so.

Preliminary insights in the device stability under illumination were inferred from MPP measurements of the device's normalized PCE over time (Fig. 3c). Since these measurements were performed in a dry room (with a relative humidity (RH) comprised between 1.6 and 2.1%), the effect of water degradation is not contemplated and only light is taken into account. The degradation rate (which is indicated by the slope of the PCE trend over time) of the standard perovskite device occurs quickly, whereas different behaviours occur for the devices with additives. Devices including a tBMPy-TFSI/perovskite layer show a reduced degradation rate compared to the undoped perovskite devices, while the addition of PVMPy-TFSI greatly decreases the rate. Furthermore, the initial effect of light is intriguing: while the pure perovskite and the perovskite with IL devices show an immediate drop of PCE when light is applied, the PIL devices show an initial increase in PCE over the first 15 seconds. This effect can be due to heat or light which can trigger the uniform diffusion of the polymer on the perovskite surface. In turn, higher ion passivation takes place inducing an improvement of the device performance after a few seconds of illumination. Because of this effect, light soaking on the PIL devices prior to *J-V* measurement, would have further increased the PCE of perovskite devices containing PVMPy-TFSI but for comparison purposes, the initial PCE was taken for all devices.

To rationalize the improvement in efficiency and light stability along with the hysteresis decrease for perovskite devices using IL and PIL additives, surface composition and energetics of the perovskite layers were investigated by X-ray and Ultra-Violet photoelectron spectroscopy (XPS/UPS), and the crystalline, optical and morphological characteristics of the perovskite layer were determined by XRD and scanning electron microscopy (SEM) analysis. The distribution of the additives at the perovskite layer surface was first evaluated by XPS spectroscopy using two modes, a conventional one (take-off angle 90°) and a more surface sensitive one (take-off angle 30°) (Fig. S17). Whatever the sample studied and the mode used, C 1s, N 1s, I 3d, I 4d, Pb 4f, Pb 5d, and Cs 3d core level binding energies were consistent with the presence of $CsFAPbI_3$ (Table S1)[51] with no evidence of metallic lead[52] and the amount of potassium was

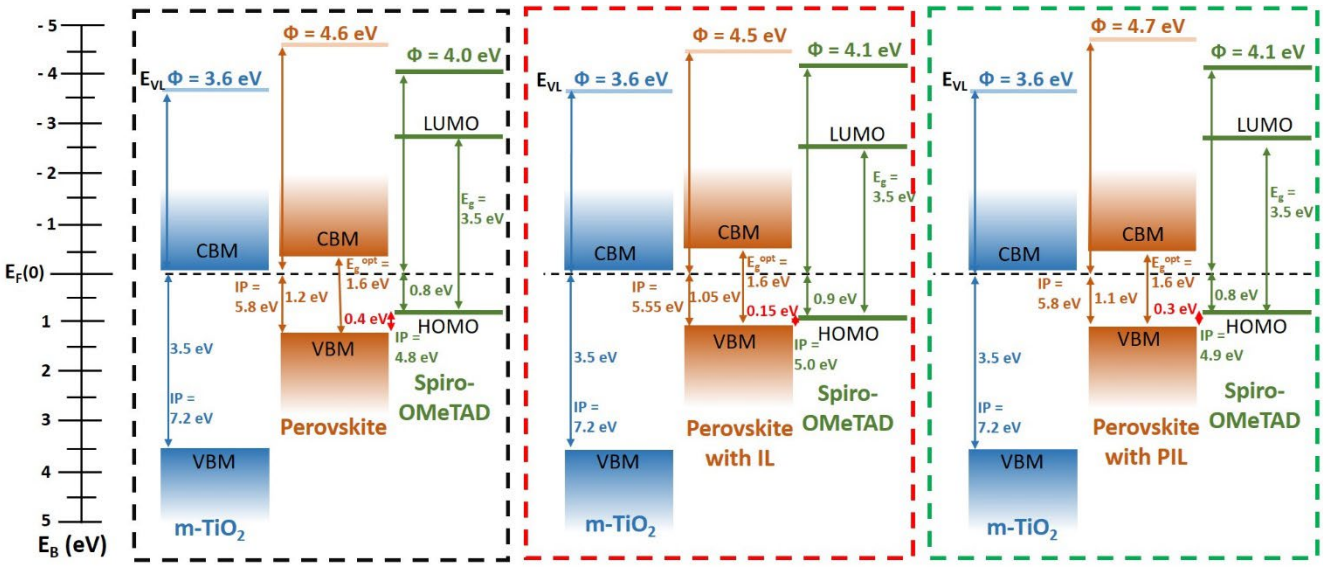

Fig. 4. Energy levels of m-TiO_2/perovskite/Spiro-OMeTAD (a) without additive, (b) with tBMPy-TFSI (IL) additive, and (c) with PVMPy-TFSI (PIL) additive.

too low to be detected. Furthermore, F1s and S2p core level features, along with an additional component in the C 1s region at 293-294 eV typical of $-CF_3$ groups, were only observed for films including additives confirming the presence of IL or PIL in the layer (Fig. S18). Moreover, according to surface stoichiometry determination (Table S2), the relative amount of fluorinated species, i.e. of additives, determined using the surface sensitive mode (take off angle of 30°) is higher for IL than for PIL additives. By contrast, the conventional mode led to a higher amount of fluorinated species in the case of PIL. A larger amount of IL than PIL was therefore located at the perovskite layer surface, i.e. at the perovskite/spiro-OMeTAD interface in PSCs, while the PIL content increases from the top of the surface to the bulk of the film. In addition, energy shifts to higher energies for core level signals (N 1s, Cs 3d, I 3d, I 4d, Pb 4f, Pb 5d) belonging to the perovskite material of 0.2 eV and 0.1 eV for the perovskite film without additive and with IL, respectively, were observed in the case of the spectra recorded for a take-off angle of 90° compared to those obtained at 30° (Fig. S19). In contrast, no energy shift was found for the perovskite film with PIL which may indicate that PIL is more localized in the bulk of the perovskite layer than IL.

Furthermore, compared to neat perovskite films that shows the expected emission bands for lead iodide perovskites,[53] UPS spectra of perovskite layers with IL or PIL additive exhibit new spectral features in the binding energy range of 6-8 and 10-12 eV that can be attributed to the pyridinium and sulfone contributions (6-8 eV) and to TFSI anion contributions (10-12 eV),[54] evidencing the presence of the additive (Fig. S20). The higher intensity of additive features in the binding energy range of 6-8 and 10-12 eV for the layers with IL also confirms a higher IL content at the surface (< 2 nm) of the perovskite film compared to the layer including PIL (Fig. S20). In addition, careful determination of the electronic parameters from the UPS spectra of the different films studied (Table S3) provides a static picture of the band alignment of the different materials making up the devices (Fig. 4). In each case, a favourable band alignment was observed, compared to the device without any additives. More interestingly, the energy difference between the valence band maximum of the perovskite and the Highest Occupied Molecular Orbital (HOMO) of spiro-OMeTAD was found to be 0.15, 0.3, and 0.4 eV for the system with IL, with PIL, and without additive, respectively. Therefore, the higher V_{OC} value found for the device involving the perovskite layer with IL additive can be attributed to the lower energy level offset for the transfer of holes from the perovskite to spiro-OMeTAD. Indeed, an increase in V_{OC} has been reported when the HOMO of the hole transporting materials is closer to the valence band

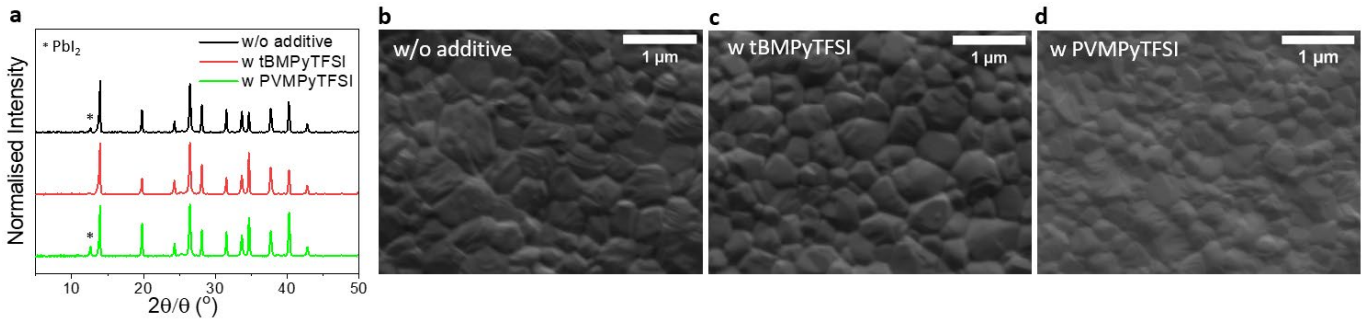

Fig. 5. Comparison between measurements on perovskite thin films without and with tBMPyTFSI and PVMPyTFSI additives, showing in a) XRD analysis performed on glass/c-TiO_2/mp-TiO_2/perovskite samples and SEM pictures of perovskite layers of b) perovskite without additive, c) with tBMPyTFSI additive and d) with PVMPyTFSI additive.

maximum of the perovskite absorber, due to rise of the built-in field and lower thermionic losses for the collected holes.[55,56]
Furthermore, XRD patterns show that the crystalline structure does not change by adding additives to the perovskite (Fig. 5a). Note that the amount of lead iodide (PbI_2) in the perovskite layer, as evidenced by the peak at 12.6° 2θ, which is attributed to (001) PbI_2, depends on the preparation conditions. Thus, the perovskite fabricated with tBMPy-TFSI exhibits no significant presence of PbI_2. By contrast, the perovskite without additive shows a small amount of precursor material while the perovskite containing PVMPy-TFSI additive exhibits a larger content in lead precursor. It is believed that PVMPy-TFSI causes the complexation of PbI_2 in the perovskite precursor, which is confirmed by the formation of smaller perovskite grains, as shown next. This complexation produces a reduction of trap states which explains the higher device performances compared to the pure perovskite devices.[57] SEM comparison between perovskite layers (pure, with IL, and with PIL) in Fig. 5b-d, shows that while tBMPy-TFSI has no significant impact on the crystal dimension, PVMPy-TFSI has. The perovskite with PIL additive produce films with smaller crystals (< 0.5 µm diameter) compared to the pure perovskite layer (*i.e.* 0.6 µm on average). Although larger grains are generally preferred to achieve longer charge diffusion lengths and increased stability, in this case the grains are slightly smaller compared to pure perovskite, but more compact and with less pronounced grain boundaries. Therefore, the passivation effects triggered by the PIL additive, compensate for the presence of smaller grains, for which the device with additives has achieved increased efficiency and stability. In addition, the improved efficiency of devices containing tBMPy-TFSI may be related to the highly oriented and compact perovskite grains, as shown in Fig. 5c, which may be a consequence of delayed crystallization during film formation. This effect is similar to the observation made by Seo *et al*., who showed that by adding methylammonium formate (MAF) IL, they obtained highly oriented and pure perovskite crystals.[25] Interestingly, when perovskite layers are exposed to light (AM1.5G) and heat (80 °C), the surface morphology shows intensive changes (Fig. S21). Nevertheless, both conditions show that bare perovskite layers undergo stronger alterations compared to IL and PIL perovskite layers, leading to significant numbers of pin-holes in the case of light exposure and loss of grain density in the case of heat.
In addition, the use of additives has an interesting effect on the surface wettability of the perovskite layer (as shown in the picture of spiro-OMeTAD deposited on perovskite films, Fig. S22). While the deposition of spiro-OMeTAD on undoped perovskite produces uniform films, the deposition becomes difficult using IL and even more complicated with PIL additives in the perovskite layer. The ionic additives change the adhesive and cohesive forces on the perovskite surface and make difficult to control the uniformity of the spiro-OMeTAD film.
In summary, all these results indicate that the improvement in V_{oc} and FF obtained with the perovskite film including IL and PIL additives is due to two main factors: a) the optimal alignment of energy levels and b) the larger amount of additive at the interface with spiro-OMeTAD. Both facilitate charge (hole) extraction/transfer over the interface with spiro-OMeTAD, the former by decreasing the energy level offset for a hole transfer to spiro-OMeTAD, and the latter by decreasing the recombination losses of the vacant sites of the perovskite at the interface with HTM producing a faster charge extraction. Furthermore, the improvement in J_{sc} determined for perovskite films with the PIL additive can be related to the distribution of the additive throughout the thin film and greater uniformity between grains that induce better passivation of defects and charge traps throughout the film, and, hence, greater mobility of charge carriers in the film. These factors also explain the better MPP tracking and lower hysteresis in *J-V* curves for devices including PIL additives, as a consequence of the better distribution of the additive in the whole film (surface and bulk), in contrast to the similar IL, which limits the ion migration processes by better passivation of the defects in both the surface and bulk.

3 Conclusions

This work introduces an original approach based on the use of PILs as additives in the perovskite absorber layer exploiting the combination of high ionic conductivity and passivation effect, due to the use of ionic liquids, within an ordered macromolecular structure. n-i-p MA-free perovskite solar cells were fabricated using tBMPy-TFSI (IL) and the novel PVMPy-TFSI (PIL) in the precursor solution, which are shown to behave as efficient quaternary ammonium additives that can passivate ionic defects at the surface and in the bulk of the perovskite layer.[15]
Although the addition of IL gave the best device performances (due to the known effect of reducing recombination losses at the interface and more favourable energy alignment), the PIL/perovskite devices are hysteresis-free and preliminary stability studies reveal greater resilience towards light compared to undoped perovskite or perovskite with IL additive, confirming that poly(ionic liquids) are highly conductive, as ILs, but more stable.[39]
According to studies performed to understand the effect of these additives on the perovskite layer, the perovskite/spiro-OMeTAD interface is richer in IL than PIL while PIL is more localized in the bulk of the perovskite film. Moreover, PILs act on the perovskite grain formation and passivation: PVMPy-TFSI/perovskites show smaller grains (< 0.5 µm) but the passivation of the grains reduces charge recombination effects and induces faster charge transport, which in turn improves the device performances and gives good prospects for improved stability of the perovskite film. Thus, uncoordinated surface states may be passivated by PIL, contributing to reduced radiative recombination losses and ion migration, which in turn reduces the solar cell hysteresis. Furthermore, especially in the case of PILs, the macromolecular structure can create a protection of the grain boundary, without affecting the light-absorbing properties of the perovskite. In this way, the grains can be protected from external agents (*i.e.* H_2O) resulting in better device stability. Indeed, the hydrophobic nature of these additives is a clear advantage against the perovskite

degradation caused by moisture, which is a detrimental factor for the device lifetime.

Finally, this study opens new avenues to improve the stability of perovskite solar cells and further analysis will be performed using IL and PIL by monitoring the stability of the device over time and under operational stress conditions (AM1.5, 85% RH, 85 °C).

Author Contributions

S. M. developed the concept of the research study, performed the experiments on the solar cells, analyzed the results, constructed the figures and prepared the manuscript draft. **D. M.** synthesized and characterized the ionic and poly(ionic liquid)s. **S. A.** and **T. B.** established the procedure for the fabrication of lead-free perovskite solar cells. **T. B.** and **M. F.** performed and analyzed the SEM and XRD experiments. **M. I.** performed and analysed the photoelectron spectroscopy characterizations. **G. H.** and **H. S.** provided funding for the study. **E. C.** and **T.T.** supervised the work, interpreted the data and reviewed the manuscript. All authors have given approval for the final version of the manuscript.

Conflicts of interest

There are no conflicts to declare.

Acknowledgments

We would like to acknowledge the LabEx AMADEUS ANR-10-LABEX-0042-AMADEUS, the program of Excellence Initiative IdEx ANR-10-IDEX-003-02, the University of Bordeaux, the Region Nouvelle Aquitaine, and the LCPO-Arkema INDUSTRIAL CHAIR "HOMERIC" ANR-13-CHIN-0002-01 for financial support. This work was also performed within the framework of the Equipex ELORPrintTec ANR-10-EQPX-28-01." In addition, we would like to thank CNRS INSIS and INC. This work was performed within LIA ' NextPV' CNRS-RCAST from Univ. of Tokyo – Segawa Lab. The authors thank the New Energy and Industrial Technology Development Organization (NEDO) PV R&D programs (No. 200015) and Ministry of Economy, Trade, and Industry in Japan for their financial supports. We would also like to thank Dr. Ludmila Cojocaru for her meaningful suggestions and strong support.

Notes and references

1 A. Kojima, K. Teshima, Y. Shirai and T. Miyasaka, *J. Am. Chem. Soc.*, 2009, **131**, 6050.
2 M. A. Green, A. Ho-Baillie and H. J. Snaith, *Nat. Photonics*, 2014, **8**, 506.
3 J. Jeong, M. Kim, J. Seo, H. Lu, P. Ahlawat, A. Mishra, Y. Yang, M. A. Hope, F. T. Eickemeyer, M. Kim, Y. J. Yoon, I. W. Choi, B. P. Darwich, S. J. Choi, Y. Jo, J. H. Lee, B. Walker, S. M. Zakeeruddin, L. Emsley, U. Rothlisberger, A. Hagfeldt, D. S. Kim, Michael Grätzel and J. Y. Kim, *Nature*, 2021, **592**, 381.
4 H. Min, D. Y. Lee, J. Kim, G. Kim, K. S.Lee, J. Kim, M. J. Paik, Y. K. Kim, K. S. Kim, M. G. Kim, T. J. Shin and S. I. Seok, *Nature*, 2021, **598**, 444.
5 https://www.nrel.gov/pv/cell-efficiency.html.
6 A. Uddin, M. B. Upama, H. Yi and L. Duan, *Coatings*, 2019, **9**, 65.
7 T. Matsui, T. Yamamoto, T. Nishihara, R. Morisawa, T. Yokoyama, T. Sekiguchi and T. Negami, *Adv. Mater.*, 2019, **31**, 1806823.
8 M M. Tavakoli, M. Saliba, P. Yadav, P. Holzhey, A. Hagfeldt, S. M. Zakeeruddin and M. Grätzel, *Adv. Energy Mater.*, 2019, **9**, 1802646.
9 J. Kim, A. Ho-Baillie and S. Huang, *Sol. RRL*, 2019, **3**, 1800302.
10 I. Jeong, J. W. Jo, S. Bae, H. J. Son and M. J. Ko, *Dyes Pigm.*, 2019, **164**. 1.
11 Y. Wang, Y. Hu, D. Han, Q. Yuan, T. Cao, N. Chen, D. Zhou, H. Cong and L. Feng, *Org. Electron.*, 2019, **70**, 63.
12 S. Wang, Z. Huang, X. Wang, Y. Li, M. Günther, S. Valenzuela, P. Parikh, A. Cabreros, W. Xiong and Y. S. Meng, *J. Am. Chem. Soc.*, 2018, **140**, 16720.
13 N. D. Pham, J. Shang, Y. Yang, M. T. Hoang, V. T. Tiong, X. Wang, L. Fan, P. Chen, L. Kou, L. Wang and H. Wang, *Nano Energy*, 2020, **69**, 104412.
14 G. Ren, W. Han, Y. Deng, W. Wu, Z. Li, J. Guo, H. Bao, C. Liu and W. Guo, *J. Mater. Chem. A*, 2021, **9**, 4589.
15 C. Pereyra, H. Xie and M. Lira-Cantu, *J. Ener. Chem.*, 2021, **60**, 599-634.
16 X. Li, M. Ibrahim Dar, C. Yi, J. Luo, M. Tschumi, S. M. Zakeeruddin, M. K. Nazeeruddin, H. Han and M. Grätzel, *Nat. Chem.*, 2015, **7**, 703.
17 N. K. Noel, A. Abate, S. D. Stranks, E. S. Parrott, V. M. Burlakov, A. Goriely and H. J. Snaith, *ACS Nano*, 2014, **8**, 9815.
18 S. Yang, Y. Wang, P. Liu, Y. B. Cheng, H. J. Zhao and H. G. Yang, *Nat. Energy*, 2016, **1**, 1.
19 Z. Wu, M. Jiang, Z. Liu, A. Jamshaid, L. K. Ono and Y. Qi, *Adv. Energy Mater.*, 2020, **10**, 1903696.
20 T. Niu, L. L. Chao, W. Gao, C. Ran, L. Song, Y. Chen, L. Fu and W. Huang, *ACS Energy Lett.*, 2021, **6**, 1453.
21 S. Ghosh and T. Singh, *Nano Energy*, 2019, **63**, 103828.
22 T. H. Schloemer, J. A. Christians, J. M. Luther and A. Selinger, *Chem. Sci.*, 2019, **10**, 1904.
23 Z. Hawash, L. K. Ono and Y. Qi, *Adv. Mater. Interfaces*, 2018, **5**, 1700623.
24 M. Shahiduzzaman, K. Yamamoto, Y. Furumoto, T. Kuwabara, K. Takahashi and T. Taima, *RSC Adv.*, 2015, **5**, 77495.
25 J. Y. Seo, T. Matsui, J. Luo, J. P. Correa-Baena, F. Giordano, M. Saliba, K. Schenk, A. Ummadisingu, K. Domanski, M. Hadadian, A. Hagfeldt, S. M. Zakeeruddin, U. Steiner, M. Grätzel and A. Abate, *Adv. Energy Mater.*, 2016, **6**, 1600767.
26 S. Bai, P. Da, C. Li, Z. Wang, Z. Yuan, F. Fu, M. Kawecki, X. Liu, N. Sakai, J. T. W. Wang, S. Huettner, S. Buecheler, M. Fahlman, F. Gao and H. J. Snaith, *Nature*, 2019, 571, 245.
27 M. Salado, F. J. Ramos, V. M. Manzanares, P. Gao, M. K. Nazeeruddin, P. J. Dyson and S. Ahmad, *ChemSusChem*, 2016, **9**, 2708.
28 Y. Zhang, Z. Fei, P. Gao, Y. Lee, F. F. Tirani, R. Scopelliti, Y. Feng, P. J. Dyson and M. K. Nazeeruddin, *Adv. Mater.*, 2017, **29**, 1702157.
29 D. Bi, P. Gao, R. Scopelliti, E. Oveisi, J. Luo, M. Grätzel, A. Hagfeldt and M. K. Nazeeruddin, *Adv. Mater.*, 2016, **28**, 2910.
30 L. Wang, Q. Miao, Z. Sun, H. Zhang, Z. Liu, G. Wang and S. Zhang, *ACS Appl. Energy Mater.*, 2021, **4**, 12112.
31 M. Peng, W. Dai, L. Lin, B. Xiao, S. Guo, M. Fang, H. Wang, Y. Gou, M. S. Irshad, J. Gong, Q and J. Li, *ACS Appl. Energy Mater.*, 2021, **4**, 12421.
32 Y. Huang, H. Zhong, W. Li, D. Cao, Y. Xu, L. Wan, X. Zhang, X. Zhang, Y. Li, X. Ren, Z. Guo, X. Wang, D. Eder and S. Wang, *Sol. Energy*, 2022, **231**, 1048.

33 C. Y. Chang, C. Y. Chu, Y. C. Huang, C. W. Huang, S. Y. Chang, C. A. Chen, C. Y. Chao and W. F. Su, *ACS Appl. Mater. Interfaces*, 2015, **7**, 4955.
34 D. Bi, C. Yi, J. Luo, J. D. Décoppet, F. Zhang, S. M. Zakeeruddin, X. Li, A. Hagfeldt and M. Grätzel, *Nat. Energy*, 2016, **1**, 16142.
35 L. Zuo, H. Guo, D. W. DeQuilettes, S. Jariwala, N. De Marco, S. Dong, R. DeBlock, D. S. Ginger, B. Dunn, M. Wang and Y. Yang, *Sci. Adv.*, 2017, **3**, e1700106.
36 B. Chaudhary, A. Kulkarni, A. K. Jena, M. Ikegami, Y. Udagawa, H. Kunugita, K. Ema and T. Miyasaka, *ChemSusChem*, 2017, **10**, 2473.
37 T. H. Han, J. W. Lee, C. Choi, S. Tan, C. Lee, Y. Zhao, Z. Dai, N. De Marco, S. J. Lee, S. H. Bae, Y. Yuan, H. M. Lee, Y. Huang and Y. Yang, *Nat. Commun.*, 2019, **10**, 520.
38 S. Wang, B. Yang, J. Han, Z. He, T. Li, Q. Cao, J. Yang, J. Suo, X. Li, Z. Liu, S. Liu, C. Tang and A. Hagfeldt, *Energy Environ. Sci.*, 2020, **13**, 5068.
39 D. Mecerreyes, *Prog. Polym. Sci.*, 2011, **36**, 1629.
40 J. Yuan and M. Antonietti, *Polymer*, 2011, **52**, 1469.
41 C. Geffroy, E. Grana, T. Bessho, S. Almosni, Z. Tang, A. Sharma, T. Kinoshita, F. Awai, E. Cloutet, T. Toupance, H. Segawa and G. Hadziioannou, *ACS Appl. Energy Mater.*, 2020, **3**, 1393.
42 P. Caprioglio, D. S. Cruz, S. Caicedo-Davila, F. Zu, A. A. Sutanto, F. Pena-Camargo, L. Keselmann, D. Meggiolaro, L. Gregori, C. M. Wolff, B. Stiller, L. Perdigon-Toro, H. Köbler, B. Li, E. Gutierrez-Partida, I. Lauermann, A. Abate, N. Koch, F. De Angelis, B. Rech, G. Grancini, D. Abou-Ras, M. K. Nazeeruddin, M. Stolterfoht, S. Albrecht, M. Antonietti and D. Neher, *Energy Environ. Sci.*, 2021, **14**, 4509.
43 Z. Tang, T. Bessho, F. Awai, T. Kinoshita, M. M. Maitani, R. Jono, T. N. Murakami, H. Wang, T. Kubo, S. Uchida and H. Segawa, *Sci. Rep.*, 2017, **7**, 12183.
44 Y. Liu, Z. Wu, Y. Dou, J. Zhang, T. Bu, K. Zhang, D. Fang, Z. Ku, F. Huang, Y.-B. Cheng and J. Zhong, *J. Phys. Chem. C*, 2020, **124**, 12249.
45 Y. Liu, S. Akin, A. Hinderhofer, F. T. Eickmeyer, H. Zhu, J.-Y. Seo, J. Zhang, F. Schreiber, H. Zhang, S. M. Zakeeruddin, A. Hagfledt, M. I. Dar and M. Grätzel, *Angew. Chem. Int. Ed.*, 2020, **59**, 15688.
46 X. Zheng, B. Chen, J. Dai, Y. Fang, Y. Bai, Y. Lin, H. Wei, X. C. Zeng and J. Huang, *Nat. Ener.*, 2017, **2**, 17102.
47 R. Marcilla, J. A. Blazquez, R. Fernandez, H. Grande, J. A. Pomposo and D. Mecerreyes, *Macromol. Chem. Phys.*, 2005, **206**, 299.
48 B. Chen, P. N. Rudd, S. Yang, Y. Yuan and J. Huang, *Chem. Soc. Rev.*, 2019, **48**, 3842.
49 D. H. Kang and N. G. Park, *Adv. Mater.*, 2019, **31**, 1805214.
50 P. Calado, A. M. Telford, D. Bryant, X. Li, J. Nelson, B. C. O'Regan and P. R. F. Barnes, *Nat. Commun.*, 2016, **7**, 13831.
51 T. J. Jacobsson, J.-P. Correa-Baena, E. H. Anaraki, B. Philippe, S. D. Stranks, M. E. F. Bouduban, W. Tress, K. Schenk, J. Teuscher, J.-E. Moser, H. Rensmo, and A. Hagfeldt, *J. Am. Chem. Soc.*, 2016, **138**, 10331.
52 B. Philippe, B.-W. Park, R. Lindblad, J. Oscarsson, S. Ahmadi, E. M. J. Johansson and H. Rensmo, *Chem. Mater.*, 2015, **27**, 1720.
53 B. Philippe, T. J. Jacobsson, J.-P. Correa-Baena, N. K. Jena, A. Banerjee, S. Chakraborty, U. B. Cappel, R. Ahuja, A. Hagfeldt, M. Odelius and H. Rensmo, *J. Phys. Chem. C*, 2017, **121**, 26655.
54 O. Höfft, S. Bahr, M. Himmerlich, S. Krischok, J. A. Schaefer and V. Kempter, *Langmuir*, 2006, **22**, 7120.
55 D. Ompong and J. Singh, *Org. Electronics*, 2018, **63**, 104.
56 W. Yan, Y. Li, S. Ye, Y. Li, H. Rao, Z. Liu, S. Wang, Z. Bian and C. Huang, *Nano Res.*, 2016, **9**, 1600.
57 R. Mastria, S. Colella, A. Qualtieri, A. Listorti, G. Gigli and A. Rizzo, *Nanoscale*, 2017, **9**, 3889.

Graphical Abstract